**The Impact of Initial Abundances on Modeling the Weak s-Process**

## Introduction

This research was done to determine the possible impacts of initial isotopic abundances on the structure and nucleosynthesis of a star, using two different models for initial isotopic abundances. The focus of this analysis was the weak s-process. The weak s-process is a neutron capture process responsible for nucleosynthesis beyond the iron peak, occurs in massive stars, and its products depend on both the available isotopes and the structure of the star. The weak s-process occurs primarily in the carbon shell of massive stars, but there is some weak s-process production during helium core burning as well (Pignatari et al, 2010). This paper will begin with discussing which stars the weak s-process occurs in, how the structure of those stars can influence the weak s-process, and how the burning stages of those stars influence weak s-process production.

The weak s-process occurs in massive stars, of about $12M_{\odot}$, with $1M_{\odot}$ being the mass of the Sun. Stars begin nucleosynthesis by burning hydrogen in the core, and stars of sufficient mass contract after finishing core hydrogen burning, causing the core to reach the temperatures necessary for core helium burning (Iliadis, 2015). The same process continues for stars of sufficient mass, as they contract after core helium burning to reach the temperatures necessary for core carbon burning. Each time these contractions occur, not all of the star contracts enough to burn the new fuel, meaning that each contraction leaves a shell from the previous burning stage, which uses the fuel of that burning stage, and is located outside of the core of the star (Iliadis, 2015). These layers of shells from earlier burning stages are important for the weak s-process, as the majority of the weak s-process takes place in the carbon shell, leftover from contractions after carbon core burning.

Carbon core burning is the third core burning phase, after hydrogen core burning and helium core burning. During a star's burning phases, nucleosynthesis can be divided into primary and secondary processes. Primary processes use hydrogen and helium for nucleosynthesis, and primary process isotope abundances scale linearly with metallicity. Secondary processes use primary process isotopes for nucleosynthesis, meaning that secondary process isotope abundances scale quadratically with metallicity. Core burning phases are primary processes, whereas the s-process and its weak component are secondary processes. Helium core burning and carbon core burning are the primary processes that are relevant to discuss for the weak-s process, as are the CNO cycles, which alter abundances before core helium burning.

Leading up to helium core burning in massive stars are the CNO cycles, which rearrange the abundance of C, N, and O, mostly into $^{14}N$. The increased $^{14}N$

abundance from the CNO cycles is important for the weak s-process due to the reactions $^{14}N$ is involved in during helium burning, which will be discussed after the CNO cycles. There are four different CNO cycles, each of which is a reaction chain. The CNO1 reaction chains are below.

1. $^{12}C(p,\gamma)^{13}N(\beta^{+}\nu)^{13}C(p,\gamma)^{14}N(p,\gamma)^{15}O(\beta^{+}\nu)^{15}N(p,\alpha)^{12}C$
2. $^{14}N(p,\gamma)^{15}O(\beta^{+}\nu)^{15}N(p,\gamma)^{16}O(p,\gamma)^{17}F(\beta^{+}\nu)^{17}O(p,\alpha)^{14}N$
3. $^{15}N(p,\gamma)^{16}O(p,\gamma)^{17}F(\beta^{+}\nu)^{17}O(p,\gamma)^{18}F(\beta^{+}\nu)^{18}O(p,\alpha)^{15}N$
4. $^{16}O(p,\gamma)^{17}F(\beta^{+}\nu)^{17}O(p,\gamma)^{18}F(\beta^{+}\nu)^{18}O(p,\gamma)^{19}F(p,\alpha)^{16}O$

$^{12}C$, $^{14}N$, and $^{16}O$ are the primary seeds for these reactions, as the $^{15}N$ abundance is expected to be significantly smaller in most cases, and in some cases the dominant reaction involving $^{15}N$ is the $^{15}N(p,\alpha)^{12}C$ reaction (Iliadis, 2015). These reaction chains do not always go to completion, leading to small abundances of isotopes other than $^{14}N$ prior to helium burning.

Helium burning begins with the triple alpha reaction chain: $^{4}He(\alpha,\gamma)^{8}Be(\alpha,\gamma)^{12}C$. $^{8}Be$ is an unstable isotope, so $^{8}Be$ production must satisfy the equation below for the $^{8}Be(\alpha,\gamma)^{12}C$ reaction to proceed.

5. $$^{4}He + {}^{4}He \leftrightarrow {}^{8}Be$$

The triple alpha reaction rates have not been measured directly in experiments yet, and as such the reaction rates depend on indirect measurements with an uncertainty of about 15% (Iliadis, 2015).

The following alpha particle reactions in hydrostatic helium burning are: $^{12}C(\alpha,\gamma)^{16}O(\alpha,\gamma)^{20}Ne$. In contrast to the 15% uncertainties in the triple alpha reaction rates, the $^{12}C$ to $^{16}O$ reaction rates have uncertainties around 35% (Iliadis, 2015). Burning stages past helium burning rely on $^{12}C$, and later $^{16}O$ as fuel, so the uncertainty in these reaction rates impacts models of the evolution of a star past this point. The $^{12}C(\alpha,\gamma)^{16}O(\alpha,\gamma)^{20}Ne$ reaction chain is relatively slow, as substantial amounts of $^{12}C$ and $^{16}O$ remain after hydrostatic helium burning, and thus are not fully used in the $^{12}C(\alpha,\gamma)^{16}O(\alpha,\gamma)^{20}Ne$ reaction chain. The $^{20}Ne$ produced can also form $^{24}Mg$ in the $^{20}Ne(\alpha,\gamma)^{24}Mg$ reaction.

Aside from reactions using exclusively $^{4}He$ nuclei, there are helium burning reactions using isotopes left from hydrostatic hydrogen burning. Leftover $^{14}N$ can participate in the $^{14}C(\alpha,\gamma)^{18}F(\alpha,\gamma)^{22}Ne$ reaction chain, which branches into either the $^{22}Ne(\alpha,\gamma)^{26}Mg$ or $^{22}Ne(\alpha,n)^{25}Mg$ reaction. During shell burning, $^{18}O$ can also participate in the $^{18}O(p,\alpha)^{15}N(\alpha,\gamma)^{19}F$ reaction chain (Iliadis, 2015).

In a large enough star, when the star no longer has enough helium to use as fuel, the star contracts until it becomes hot enough to use carbon as fuel. Carbon burning primarily uses $^{12}C$ from helium burning as fuel. In carbon burning, most

reactions will use $^{12}C$ or $^{16}O$, which are the most common elements left over from helium burning. Relevant $^{12}C$ reactions are $^{12}C(^{12}C,p)^{23}Na$, $^{12}C(^{12}C,\alpha)^{20}Ne$, $^{12}C(^{12}C,n)^{23}Mg$, $^{12}C(^{12}C,\gamma)^{24}Mg$, and $^{12}C(^{12}C,^{8}Be)^{16}O$ (Iliadis, 2015). Isotopes can also absorb protons and undergo gamma decay, or absorb alpha particles and undergo neutron decay, but these processes are less common in core burning than in shell burning and are typically part of a reaction chain leading to $^{23}Na$, $^{26}Mg$, or the $^{13}C(\alpha,n)^{16}O$ reaction. The small number of free protons, neutrons, and alpha particles means that the $^{12}C$ and $^{16}O$ fusion reactions are dominant (Iliadis, 2015).

Once a star progresses through carbon core burning, and has a carbon shell, the energy transfer method of the carbon shell, as well as its distance from the core of the star, are important in determining weak s-process isotope production (Pignatari et al, 2010). Energy transfer in the carbon shell can be convective or radiative, but need not be entirely one or the other. In convective energy transfer, material deeper in the star, that is surrounded by heavier isotopes, moves upwards. This upwards movement stops when the material is surrounded by isotopes of the same weight, and this movement of material can bring energy or light nuclei needed for a particular process (Steinkirch, 2012). Whether a carbon shell is more or less convective depends on the star's initial abundances. Changes in the abundance of carbon in the core after helium burning can impact the structure of the star and later nucleosynthesis stages, such as causing a more convective carbon shell. (West, Heger, and Austin, 2013). The distance of the carbon shell from the core of the star is relevant for stars that become supernovae. When a star becomes a supernova, both energy and material from the core of the star move out through the rest of the star, which can alter the isotopes that those materials encounter. A carbon shell closer to the center of a star will have its weak s-process products be altered more during a supernova than a carbon shell further from the center of the star (Iliadis, 2015). This means that stars with a carbon shell closer to their center will release fewer weak s-process products into the interstellar medium in the case of a supernova, because those weak s-products will be altered more by that supernova.

There are core burning stages beyond carbon core burning, which is the last stage of core burning for stars around 10 times the mass of the sun, but not for larger stars. Neon is the next fuel for stars after carbon, because neon will photodisintegrate in a star sooner than oxygen due to neon's lower alpha particle separation energy. This leads to alpha particle reactions with existing nuclei, primarily producing magnesium and silicon. Following neon burning, oxygen burning occurs. The most abundant isotopes during oxygen burning are $^{16}O$, $^{24}Mg$. and $^{28}Si$ (Illiadis, 2015). The last core burning stage a star can reach is silicon burning. The most abundant isotopes during silicon burning are $^{28}Si$ and $^{32}S$, which do not fuse together, but instead undergo photodisintegration similarly to neon burning, but with a greater variety of products. After silicon burning, the

most abundant isotopes, listed in order of abundance, are $^{56}$Fe, $^{52}$Cr, $^{54}$Fe, $^{55}$Fe, and $^{53}$Mn, though $^{55}$Fe is unstable (Iliadis, 2015). These isotopes are then used as seed nuclei for other processes that occur during shell burning or alongside core burning, as when a star dies, these heavy seed nuclei can become a part of the interstellar medium, and become part of a newly born star's initial abundances.

**The s-Process**

The s-process is responsible for producing isotopes beyond $^{56}$Fe, making stable isotopes between $57<A<209$. The main s-process occurs in the helium shell of asymptotic giant branch stars (AGB). Dredge ups where material from the core of the star is ejected into its shell provide the necessary seed nuclei and neutrons to the helium shell of the AGB stars (Gallino et al, 1998, Iliadis, 2015). Whereas core burning is a primary process, all three components of the s-process are secondary processes. Thermal pulses from the AGB stars move material that has already undergone the main s-process back into the core of the star, and inject fresh seed nuclei and neutron sources into the helium shell of the star, which allows for the main s-process to continue. The abundance of isotopes produced in the main s-process is highly dependent on the abundance of $^{13}$C in the helium shell. The $^{13}$C used in the main s-process is largely produced by the $^{12}C(n,\gamma)^{13}C$ reaction (Gallino et al, 1998, Iliadis, 2015). The s-process is divided into the weak s-process, the main s-process which produces isotopes from iron until lead, and the strong s-process which produces $^{208}$Pb.

In the s-process, seed nuclei, neutron source, and neutron poison concentrations all determine the amount of s-process isotopes produced. Seed nuclei are isotopes that are often already present in a star, having been synthesized by an earlier star that ejected the material. These isotopes are the end products of silicon burning, listed in order of abundance: $^{56}$Fe, $^{52}$Cr, $^{54}$Fe, $^{55}$Fe, and $^{53}$Mn (Iliadis, 2015). The seed nuclei absorb neutrons until the nucleus becomes unstable, at which point the nucleus undergoes beta decay until it reaches a stable state as a different element. The s-process is considered slow because the rates of neutron and beta decay during this process of neutron absorption are high enough that seed nuclei often decay back into their initial state rather than reach a different stable isotope. The equation below describes the abundance evolution of an s-process product with no unstable isotopes along its s-process path. A is the atomic mass of the isotope, $N_n$ is the number density of free neutrons, $N_s(A)$ is the number density of nuclei with atomic mass A, and $\langle\sigma v\rangle_A$ is the neutron capture rate per particle pair of the nucleus with atomic number A.

6. $$\frac{dN_s(A)}{dt} = -N_n N_s(A)\langle\sigma v\rangle_A + N_n N_s(A-1)\langle\sigma v\rangle_{A-1}$$

The isotopes involved in neutron producing reactions relevant for the s-process are neutron sources, most commonly $^{13}C$ and $^{22}Ne$. The dominant neutron source reactions for the weak s-process are $^{13}C(\alpha,n)^{16}O$ and $^{22}Ne(\alpha,n)^{25}Mg$ (Iliadis, 2015, Pignatari et al, 2010). S-process reactions require large amounts of neutrons to reach heavier isotopes than iron due to the high beta decay rates, so a large abundance of neutron sources and a small abundance of seed nuclei ensures that seed nuclei are more likely to absorb multiple neutrons before decaying. Neutron poisons are isotopes that participate in reactions that require neutrons or that absorb alpha particles without undergoing neutron decay. These isotopes compete with neutron sources for alpha particles and with seed nuclei for neutrons. $^{16}O$, $^{22}Ne$, and $^{25}Mg$ are notable neutron poisons for the weak s-process, involved in the following reactions: $^{16}O(n,\gamma)^{17}O(\alpha,\gamma)^{21}Ne$, $^{22}Ne(n,\gamma)^{23}Ne$, $^{25}Mg(n,\gamma)^{26}Mg$ (Pignatari et al, 2010, Rayet and Hashimoto, 1999).

The s-process is the only source of six isotopes: $^{70}Ge$, $^{76}Se$, $^{80}Kr$, $^{82}Kr$, $^{86}Sr$, and $^{87}Sr$. The weak s-process occurs during core helium burning and during convective shell carbon burning, and the weak s-process contribution to the abundances of the six s-process only isotopes can be isolated easily using solar decomposition fractions, which represent the fraction of that isotope's abundance came from the weak s-process, specifically for the sun (Pignatari et al, West and Heger 2013). As part of the s-process, weak s-process reaction chains would look like:

7. $$^{56}Fe(n,\gamma)^{57}Fe(n,\gamma)^{58}Fe(n,\gamma)^{59}Fe(\beta^{+}\nu)^{59}Co(n,\gamma)^{60}Co(\beta^{+}\nu)^{60}Ni$$

where the seed nucleus captures neutrons until it becomes unstable, and beta decays once it becomes unstable from absorbing neutrons (Iliadis, 2015). The weak s-process is weak because once a seed nucleus becomes unstable, the beta decay rates are much greater than the neutron capture rates for most of the weak s-process. There are points in the weak s-process where these two rates are close, leading to a branching structure for those reactions, where the nucleus could either undergo beta decay or absorb another neutron. The branching ratio equations are below, with $N_s(A)$ referring to the number density of nuclei with atomic mass A, $\tau$ refers to neutron exposure, $\sigma$ refers to the neutron capture rate for the isotope, $\lambda_\beta$ refers to the beta decay rate and $\lambda_{n\gamma}$ refers to the neutron capture rate.

8. $$B \equiv (N_s(A, \tau)\langle\sigma\rangle_A) / (N_s(A + 1, \tau)\langle\sigma\rangle_{A+1}) = \lambda_\beta(A') / (\lambda_\beta(A') + \lambda_{n\gamma}(A'))$$

To model initial abundances accurately for stellar simulations, which simulate the evolution of a star until it becomes a supernova, the initial abundance models must take into account which isotopes are produced in primary and

secondary processes. One model currently used to determine these initial abundances is the scaled solar model, which assumes all isotopes are products of primary processes, and thus scale linearly with metallicity. Another model for initial abundances is the galactic chemical histories model, which fits observational data for isotopes to a curve, which could approximate secondary process products more accurately, as the curve fit to observational data could more accurately reflect secondary process production (West and Heger, 2013).

**Methodology**

The purpose of this research was to determine how initial isotopic abundances impact the structure and nucleosynthesis of a star. These initial isotopic abundances are altered during a star's life, and become a part of the interstellar medium, mixing isotopes deposited by other stars, and becoming part of a new generation of stars. Tracking the development of these abundances throughout generations of stars is difficult, and even tracking changes in abundances for a single star is difficult, given that not all of the initially present isotopes are altered before becoming part of the interstellar medium. Further complicating this research is that for analyzing stars other than the sun, the abundance data will be for elements, rather than isotopes. In this research, two different models of initial isotopic abundances were fed into stellar simulations and GCE models, after which the differences in outputs could be compared. The differences between the initial isotopic abundances are known, and when combined with differences between outputs, can provide hypotheses for how a star's structure and nucleosynthesis might be different if the initial isotopic abundances are altered.

Historically, stellar models have used a simple model for determining initial abundances, called the scaled solar model. This model scales solar abundances linearly with metallicity, as primary process products, which functions for most isotopes, but for the isotopes made from secondary processes, or from processes which begin after some delay, the scaled solar model serves as a poor approximation. West and Heger (2013) worked on a model that fits a curve to observational data, in order to better address secondary and delayed processes, which the fitted curve could approximate better than the scaled solar model. This research involved using both the scaled solar and galactic chemical histories model from West and Heger to produce initial abundances to be used as inputs for stellar simulations.

The abundances from the scaled solar and histories models were fed into a stellar simulation, so that the results of the stellar simulation could be fed into a GCE model, for more detailed results. The stellar simulations required an input for determining nucleosynthesis directly and for determining the structure of the star. While an actual star would not have separate abundances for determining

structure and nucleosynthesis, being able to vary these parameters separately is useful for determining what impacts structure or nucleosynthesis can have on the developing abundances of a star. The separation of the two parameters would help determine if one input model had a greater impact on a parameter than the other, by providing results where one model was used for structure, and the other model for nucleosynthesis. The two different models for initial abundances and two inputs required for the stellar simulations meant that there were four different sets of stellar simulations run, GG, SG, GS, and SS. The first letter in each data set refers to the input model used for determining nucleosynthesis directly, and the second letter refers to the input model used for determining structure. The two input models were the scaled solar model, referred to as S, and the galactic chemical histories model, referred to as G (see fig. 1). This would provide output data for each possible combination of the scaled solar and galactic chemical histories models for the stellar simulations. The stellar simulations were run for stars of 13, 15, 17, 20, 22, 25, 27, and 30$M_{\odot}$. For each mass value, the simulations were run using thirteen metallicities [Z]: 0.2, 0.1, 0, -0.1, -0.2, -0.4, -0.6, -0.8, -1, -1.5, -2, -2.5, -3, and -4. Each stellar simulation developed through hydrostatic burning until the Fe-core collapsed and reached an inward velocity of $10^8$cm $s^{-1}$(West, Heger, and Côté). The galactic chemical evolution model used the results of the stellar simulations as inputs, and simulated the expected abundances for a star with a metallicity of 0, the same metallicity as the Sun. This ensured that the results of the GCE model would be directly comparable to solar abundances, and the conformity of the results with solar abundances could be used in determining which model for initial abundances was a more accurate approximation. The result of the GCE model was four sets of abundances, which were then divided by the Lodders et al 2020 solar abundances for easier comparison.

| | | Nucleosynthesis | |
|---|---|---|---|
| | | Galactic Model | Scaled Solar |
| Structure | Galactic Model | GG | SG |
| | Scaled solar | GS | SS |

Fig.1 : The input model combinations for the initial compositions of the stellar simulations. The first letter is the input model for nucleosynthesis, and the second letter is the input model for structure. (figure from West, Heger, and Côté)

The abundance ratios from the GCE model were compared for the six s-process only isotopes, due to this paper's focus on the weak s-process, though ideally an analysis of all 287 stable isotopes would be conducted. The six isotopes were chosen as indicators of whether the scaled solar or histories model would lead to more accurate results in the weak s-process, as the weak s-process portion of six s-process only isotopes could be isolated easily. This was done by multiplying the end abundances from the GCE model by the solar decomposition fraction for the weak s-process contribution, taken from the Lodders et al . 2009 data contained in West and Heger (2013). In order to have more available information on the differences in production of the weak-s process between the GCE results, neutron sources and poisons, as discussed in the introduction, were plotted in the same fashion as the s-process only isotopes.

The selected neutron sources were $^{12}C$, $^{13}C$, $^{14}N$, $^{18}O$, $^{21}Ne$, and $^{22}Ne$. $^{13}C$ and $^{22}Ne$ are involved in the two primary neutron producing reactions for the weak s-process, core $^{12}C$ abundances can determine how much of a star's carbon shell is convective, $^{14}N$ is involved in a neutron producing reaction, $^{18}O$ is involved in $^{22}Ne$ production, and $^{21}Ne$ is also involved in a neutron producing reaction (Iliadis, 2015, Pignatari et al, 2010).While $^{12}C$ is not involved in important neutron producing reactions, $^{12}C$ is a key component in $^{13}C$ production, which takes part in one of the two most important neutron producing reactions for the weak s-process(Iliadis, 2015).

The selected neutron poisons were $^{16}O$, $^{20}Ne$, $^{23}Na$, $^{24}Mg$, $^{25}Mg$, and $^{26}Mg$. High concentrations of $^{16}O$ can act as a strong neutron poison at low metallicities, $^{20}Ne$ can in some circumstances act as a light neutron poison, $^{23}Na$ can be an important neutron poison in the carbon shell, $^{24}Mg$ , $^{25}Mg$, and $^{26}Mg$ all take part in neutron capture reactions during the same burning stages as the weak s-process, and $^{25}Mg$ in particular has a large neutron capture cross section (Pignatari et al, 2010, Rayet and Hashimoto, 1999).

To better understand how any differences in the results of the GCE model came to be, the abundances of the histories model were divided by the abundances of the scaled solar model, and plotted for seed nuclei at [Z] = -1 and [Z] = -3. The selected neutron seeds were eight stable nuclei that are close to light weak s-process products in their number of neutrons. These potential seed nuclei were $^{52}Cr$, $^{53}Cr$, $^{54}Cr$, $^{55}Mn$, $^{54}Fe$, $^{56}Fe$, $^{57}Fe$, and $^{58}Fe$. While these nuclei may not all have large neutron capture cross sections, these nuclei require fewer neutrons captured to move beyond iron into a weak s-process product.

The initial neutron source abundances from the histories and scaled solar model were also analyzed, with the abundances of the histories model divided by the abundances of the scaled solar model, for [Z]= -1 and [Z]= -3. The selected neutron sources were $^{12}C$, $^{13}C$, $^{14}N$, $^{21}Ne$, and $^{22}Ne$. $^{18}O$ was not included in this set

of neutron sources because initial abundances of $^{18}O$ were not expected to impact the structure of the simulated stars substantially, and the already present $^{22}Ne$, rather than its production later on, is the relevant from the initial abundances.

**Results**

The results of the GCE model, for each combination of the scaled solar and histories model showed greater differences between combinations with different inputs for stellar structure than with different inputs for the initial nucleosynthesis in the six s-process only isotopes (see fig. 2). All four sets of results remained within an order of magnitude of the Lodders et al 2020 data. There was the least difference between the results for GG and SG results, which shared the histories model as an input for stellar structure, but differed in the input for initial nucleosynthesis. Despite the GS and SS results sharing the same inputs for structure, there were greater differences between these two models than between the GG and SG results. All four sets of inputs underproduced every s-process only isotope except $^{70}Ge$, which was overproduced slightly in the GG and SG results, though was still less than 1.1 times Lodders et al 2020 abundances. The GG and SG results were overall closer to solar abundances of s-process only isotopes, with the exception of $^{80}Kr$, which was underproduced in the GG and SG results by a greater margin than in the GS and SS results. The differences between GG and SG production of s-process only isotopes was negligible, but in the case of GS and SS, the SS results were notably closer to solar abundances than the GS results. Of the s-process only isotopes, neutron sources, and neutron poisons, the s-process only isotopes had the greatest range of production, from just over what was observed in Lodders et al 2020, to slightly above 0.1 times what was observed in Lodders et al 2020, varying based on isotope and the input model.

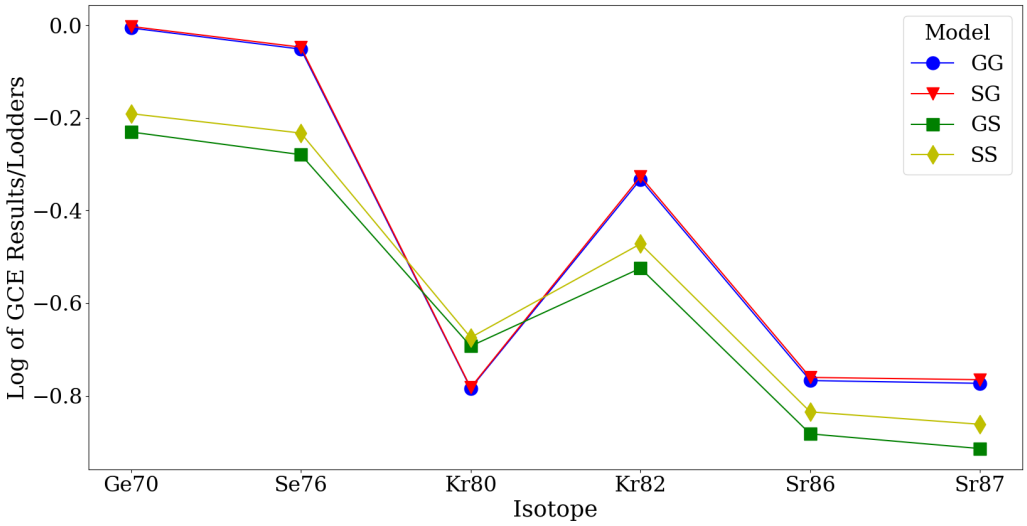


Fig. 2 This plot shows the final abundances from the GCE models for each set of initial abundances, divided by the Lodders et al 2020 solar abundances for those isotopes, and multiplied by the Lodders et al 2009 solar decomposition fractions for the weak s-process for each isotope.

The GCE model results for neutron sources were similar to the weak-s process only isotopes in that the GG and SG results were less different than the GS and SS results (see fig. 3). All four sets of results underproduced neutron sources, but remained within an order of magnitude of the Lodders et al 2020 data. The GG and SG results had lower amounts of neutron sources at the end of the GCE model than the GS and SS results, and the SS results had the greatest amount of neutron sources at the end of the GCE model.

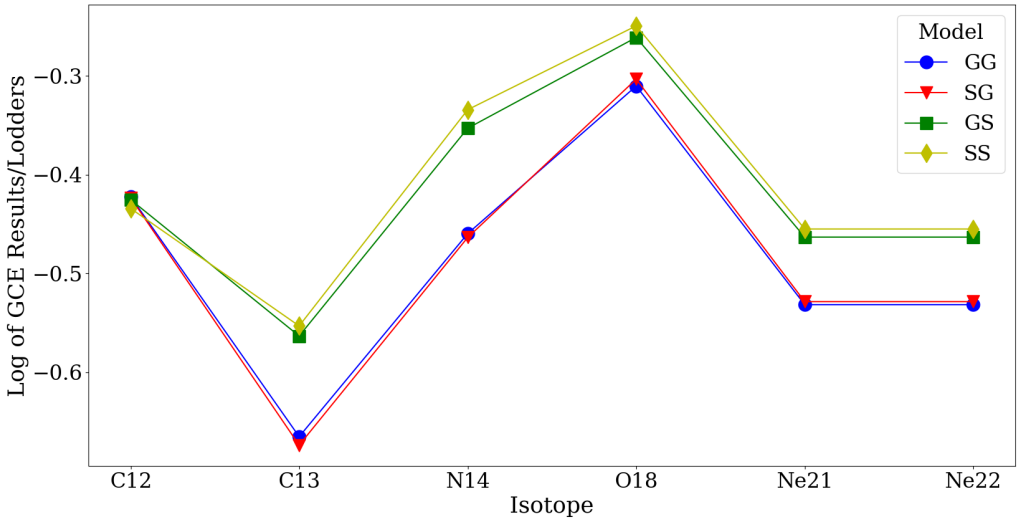


Fig. 3 This plot shows the final abundances for relevant neutron sources from the GCE model for each set of input abundances, divided by the Lodders et al 2020 abundances for each isotope.

The GCE model results for neutron poisons had all four models underproduce the neutron poisons, still within an order of magnitude of the Lodders et al 2020 data, and with one exception (see fig. 4). The GG and SG results both overproduced $^{16}O$, about 1.1 times the amount of $^{16}O$ as observed in Lodders et al 2020. The GG and SG results produced more of every neutron poison except for $^{23}Na$, though the difference between the four sets of results for $^{23}Na$ was smaller than for all neutron poisons aside from $^{12}C$. The GG and SG results remained very similar, with greater differences between the GS and SS results. Aside from $^{12}C$ and $^{20}Ne$, all neutron poisons were produced in greater ratios than neutron sources by the end of the GCE model.

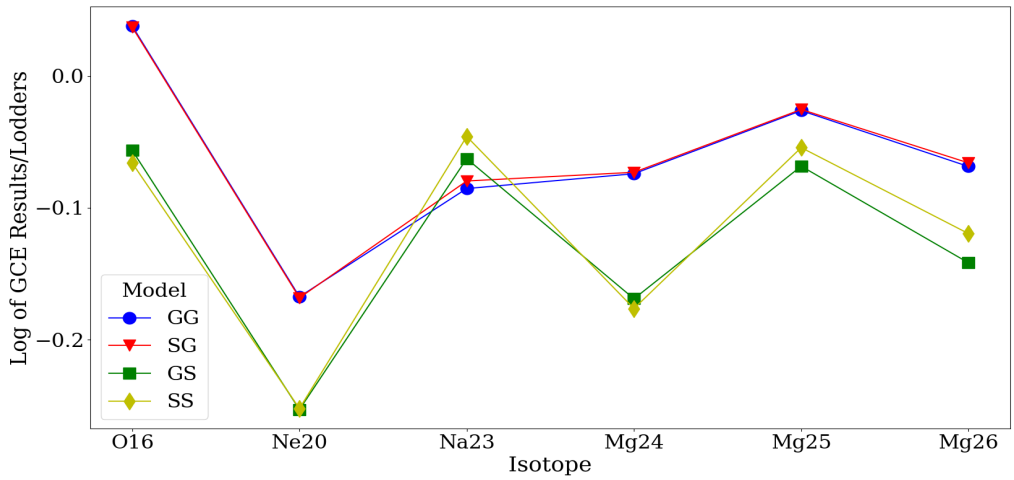


Fig. 4 This plot shows the final abundances for relevant neutron poisons from the GCE model for each set of input abundances, divided by the Lodders et al 2020 abundances for each isotope.

The initial abundances for the histories model differ substantially from the scaled solar model, both in neutron sources and in seed nuclei, especially at lower metallicity for neutron sources. At [Z] = -1 isotopes involved in neutron producing reactions were produced up to 1.5 times more in the histories model than the scaled solar model, specifically isotopes relying on products of the triple alpha reaction (see fig. 5). At [Z] = -3, these isotopes were produced between 1.5 and 4 times more in the histories model than the scaled solar model. The histories model produced less seed nuclei than the scaled solar model at both [Z] = -1 and [Z] = -3, producing up to two orders of magnitude less of some isotopes than the scaled solar model (see fig. 6). The only substantial difference in seed nucleus abundance ratios between the two metallicities was a twofold decrease in the abundance of $^{57}$Fe going from [Z] = -1 to [Z] = -3.

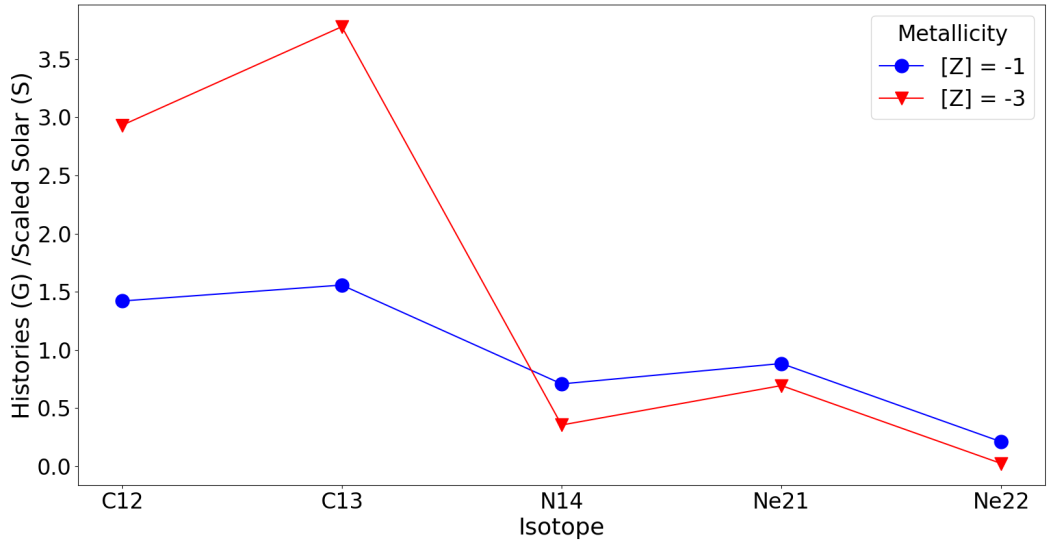


Fig. 5 This plot shows the ratio of the abundances from the galactic chemical histories model divided by the abundances from the scaled solar model, for relevant neutron sources. The abundances from the scaled solar and GCH models were used as inputs for stellar simulations.

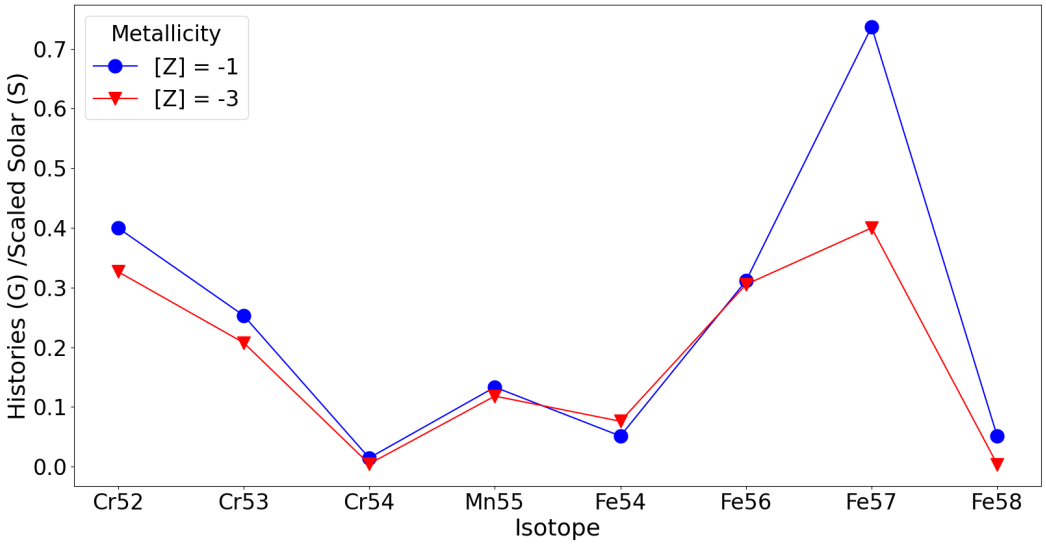


Fig. 6 This plot shows the ratio of the abundances from the galactic chemical histories model divided by the abundances from the scaled solar model, for relevant neutron sources. The abundances from the scaled solar and GCH models were used as inputs for stellar simulations.

**Discussion**

The results from the neutron sources and poisons provide possible explanations for differences in the results from the s-process only isotopes. The lower resulting abundances of neutron sources could be consistent with the hypothesis that these neutron sources were used in neutron producing reactions, and thus fewer neutron sources would remain unchanged by the end of the GCE model. The higher resulting abundances of neutron poisons could be consistent with the hypothesis that these neutron poisons are capturing fewer neutrons, and are not undergoing reactions that would alter the neutron poisons, leaving more neutron poisons unchanged at the end of the GCE model. Both of these hypotheses could help explain the greater s-process only isotope production from the weak s-process, as a larger quantity of neutrons available and fewer poisons absorbing those neutrons could lead to greater production of weak s-process isotopes. Similar hypotheses can be applied to the results with more neutron sources at the end of the GCE model, fewer neutron poisons, and lower s-process only isotope production. The greater end abundances of neutron sources could reflect fewer reactions producing neutrons involving those neutron sources. The lower end abundances of neutron poisons could reflect more neutron poisons capturing neutrons, and becoming different isotopes. Both of these hypotheses could explain lower production of weak s-process isotopes due to lower neutron availability from fewer neutron producing reactions and more competing neutron capture reactions. While the results of the GCE models are consistent with these hypotheses, that alone is insufficient to determine whether the hypotheses are correct in assuming what processes caused these differing abundances.

The differences in initial abundances between the scaled solar and histories models could support the hypotheses from the end results. The histories model had a higher initial abundance of neutron sources, and a lower initial abundance of seed nuclei when compared to the scaled solar model. The higher initial abundance of neutron sources in the histories model could lead to more neutron producing reactions, and a greater number of neutrons available for the weak s-process, which would be consistent with the results for the weak s-process contributions to the s-process only isotopes. The lower initial abundances of seed nuclei in the histories model could lead to greater production of heavier weak s-process isotopes, which require more neutrons to be captured by seed nuclei. This would be consistent with larger final abundances of the s-process only isotopes, which are relatively heavy weak s-process products.

The discussed hypotheses only extend into the possible impact of the inputs for nucleosynthesis, but do not provide an explanation for the greater impact the inputs for structure had on the weak s-process contribution to s-process only isotopes. The results of the GCE models showed that changes in the initial abundances that determine the structure and evolution of a star lead to greater

differences in the weak s-process contribution of s-process only isotopes than changes in the initial abundance used to determine isotopes available for nucleosynthesis. This could be due to increased weak s-process isotope production when the carbon shell of a star, during carbon shell burning, is convective, which would be determined by the inputs for structure. Increasing the initial abundances of carbon in a star can lead to a more convective carbon shell, and greater weak s-process isotope production (Pignatari et al, 2010, West, Heger, and Austin, 2013). The initial abundance ratios show that the histories model has a greater initial abundance of carbon, especially at low metallicities, which could cause the stellar simulations with the histories model as the input for structure to develop convective carbon shells, leading to greater weak s-process production. This would be consistent with the GCE model results, where the GCE models with the histories model as the initial input for structure had greater weak s-process contributions to all s-process only isotopes with the exception of $^{80}$Kr.

While the hypotheses discussed could be accurate, and are consistent with the results of this research, any relationship at this stage is only in correlations. Further research would be required to strengthen those correlations and determine whether the hypotheses are correct in determining the causes of differences in weak s-process production across the different initial abundances. This further work could involve analyzing isotope abundances of other secondary processes, such as the main s-process or strong s-process using the same data. Further work could also include analyzing the outputs of the stellar simulations, which were not analyzed for this paper, but are an important step between the initial isotopic abundances and the results of the GCE model. These options for future work are purely computational, but future work could also involve an observational component in collecting data to refine or create another model for determining initial isotopic abundances. Such a model could then be used for computational research similar to what was done in this paper. Future work to determine a causal relationship could involve examining the stellar simulation and GCE model code, or running the GCE model for shorter timesteps and examining the results at each timestep. This work would be computational in nature, though work regarding the particular code of the GCE model would be difficult.

**References**

Arnould, M, and Goreily, S. *The p-process of stellar nucleosynthesis: astrophysics and nuclear synthesis status*. Physics Reports Volume 384, Pages 1-84. 2013

Asplund, M, Amarsi, A. M, and Grevesse, N. *The chemical make-up of the sun: a 2020 vision*. Astronomy and Astrophysics, Manuscript. 2021.

Burbidge et al. *Synthesis of the Elements in Stars*. Reviews of Modern Physics, Volume 29, Number 4. October, 1957.

Gallino et al. *Evolution and Nucleosynthesis in Low-Mass Asymptotic Giant Branch Stars II. Neutron Capture and the s-Process*. The Astrophysical Journal, Volume 497, Pages 388-403. April 10, 1998.

Heger, Alexander, and Woosley, S. E. *Nucleosynthesis and Evolution of Metal-Free Stars*. The Astrophysical Journal, Volume 724, Number 1, Pages 341-373. November 2, 2010.

Iliadis, Christian. *Introduction to Nuclear Astrophysics*. arXiv. Nov 20, 2009. https://arxiv.org/abs/0911.3965v1

Iliadis, Christian. *Nuclear Physics of Stars*. Wiley-VCH, Weinheim, Germany. 2nd Revised and Enlarged Edition, 2015.

Pignatari et al. *The Weak s-Process in Massive Stars and its Dependence on the Neutron Capture Cross Sections*. The Astrophysical Journal, Volume 710, Number 2, Pages 1557-1577. February 1, 2010.

Prantzos, N. *Production and evolution of Li, Be, and B isotopes in the Galaxy*. Astronomy and Astrophysics, Volume 542. 2012.

Qian, R. Z, and Wasserburg, G. J. *A Model for Abundances in Metal-Poor Stars*. The Astrophysical Journal, Volume 559, Pages 925-941. October 1, 2001.

Rayet, Marc, and Hashimoto, Masa-aki. *The s-process efficiency in massive stars*. Astronomy and Astrophysics Volume 354, Pages 740-748. December 2, 1999.

Steinkirch, Marina von. *The Ledoux Criterion for Convection in a Star*. August 2, 2012

Timmes, F. X, Woosley, S. E, and Weaver, Thomas A. *Galactic Chemical Evolution: Hydrogen through Zinc*. The Astrophysical Journal Supplement Series, Volume 98, Pages 617-658. June, 1995.

Tur, Clarisse, Heger, Alexander, and Austin, Sam M. *Dependence of s-Process Nucleosynthesis in Massive Stars on Triple Alpha and $^{12}C(\alpha,\gamma)^{16}O$ Reaction Rate Uncertainties*. The Astrophysical Journal, Volume 702, Pages 1068-1077. September 10, 2009.

West, Christopher, Heger, Alexander, and Austin, Sam M. *The Impact of Helium-Burning Reaction Rates on Massive Star Evolution and Nucleosynthesis*. The Astrophysical Journal, Volume 769, Number 2. April 29, 2013.

West, Christopher, and Heger, Alexander. *Metallicity-Dependent Galactic Isotope Decomposition for Nucleosynthesis*. The Astrophysical Journal, Volume 774, Number 1. August 19, 2013.

West, Christopher, Heger, Alexander, and Côté, Benoît. *The Impact of Initial Composition on Massive Star Evolution and Nucleosynthesis*. Working Paper.